HHS Public Access

Author manuscript

Exp Neurol. Author manuscript; available in PMC 2017 April 01.

Published in final edited form as:

Exp Neurol. 2016 April ; 278: 116–126. doi:10.1016/j.expneurol.2016.02.002.

Abnormal response of distal Schwann cells to denervation in a mouse model of motor neuron disease

Dario I. Carrasco[1], **Ben A. Bahr**[3], **Kevin L. Seburn**[2], and **Martin J. Pinter**[1]

[1]Department of Physiology, Emory University, Atlanta, GA, USA

[2]The Jackson Laboratory, Bar Harbor, ME, USA

[3]Biotechnology Research and Training Center, University of North Carolina-Pembroke, Pembroke, NC, USA

Abstract

In several animal models of motor neuron disease, degeneration begins in the periphery. Clarifying the possible role of Schwann cells remains a priority. We recently showed that terminal Schwann cells (TSCs) exhibit abnormalities in postnatal mice that express mutations of the SOD1 enzyme found in inherited human motor neuron disease. TSC abnormalities appeared before disease-related denervation commenced and the extent of TSC abnormality at P30 correlated with the extent of subsequent denervation. Denervated neuromuscular junctions (NMJs) were also observed that lacked any labeling for TSCs. This suggested that SOD1 TSCs may respond differently than wildtype TSCs to denervation which remain at denervated NMJs for several months. In the present study, the response of SOD1 TSCs to experimental denervation was examined. At P30 and P60, SC-specific S100 labeling was quickly lost from SOD1 NMJs and from preterminal regions. Evidence indicates that this loss eventually becomes complete at most SOD1 NMJs before reinnervation occurs. The loss of labeling was not specific for S100 and did not depend on loss of activity. Although some post-denervation labeling loss occurred at wildtype NMJs, this loss was never complete. Soon after denervation, large cells appeared near SOD1 NMJ bands which colabeled for SC markers as well as for activated caspase-3 suggesting that distal SOD1 SCs may experience cell death following denervation. Denervated SOD1 NMJs viewed 7 days after denervation with the electron microscope confirmed the absence of TSCs overlying endplates. These observations demonstrate that SOD1 TSCs and distal SCs respond abnormally to denervation. This behavior can be expected to hinder reinnervation and raises further questions concerning the ability of SOD1 TSCs to support normal functioning of motor terminals.

Keywords

motor neuron disease; Schwann cell; neurodegeneration; motor terminal; denervation cell death

Corresponding author: Martin J. Pinter, Department of Physiology, Emory University School of Medicine, 615 Michael St., Atlanta, GA 30322, mpinter@emory.edu.

INTRODUCTION

Recent studies have drawn attention to a possible role of terminal Schwann cells (or perisynaptic Schwann cells) in the loss of innervation found in mouse models of motor neuron disease (MND). The terminal Schwann cell (TSC) is one of three cell types present at the neuromuscular junction (NMJ) and provides an intimate covering of the motor terminal. TSCs normally sense activity in motor terminals and are actively involved in modulating release of acetylcholine from motor terminals (Todd et al., 2010; Darabid et al., 2013). In mice that express the G37R mutation of the superoxide dismutase (SOD1) enzyme and develop a motor neuron disease phenotype, this signaling is found to be altered before the onset of symptoms (Arbour et al., 2015). Significant abnormalities of TSC morphology which occur before the onset of motor terminal degeneration have been recently described in G93A SOD1 mice. As many as half of fully innervated NMJs in the P30 fast medial gastrocnemius (MG) muscle lack TSCs and are instead covered by the processes of SCs located along the preterminal axon. All NMJs in the slow soleus muscle, by contrast, have one or more TSC. By P60, NMJ denervation is significantly greater in the MG than in soleus muscles demonstrating that the pattern of TSCs abnormality found at P30 is correlated with the pattern of motor terminal degeneration found at P60 (Carrasco et al., 2016). The significance of these results derives from 2 related lines of enquiry. First, in several MND animal models, motor neuron degeneration begins in the periphery (Sagot et al., 1996; Balice-Gordon et al., 2000; Fischer et al., 2004; Gould et al., 2006). Second, TSCs have a vital but poorly understood trophic relationship with motor terminals (Koirala et al., 2003; Reddy et al., 2003). An improved understanding of how TSCs are altered in MND animal models may thus provide important insights into mechanisms that produce motor terminal degeneration.

During the study of P60 SOD1 MG muscles, we noted that denervated NMJs and the surrounding preterminal regions did not show S100 immunolabeling as is commonly observed at denervated wildtype NMJs (Carrasco et al., 2016). Denervated SOD1 NMJs and surrounding preterminal regions also failed to label for P75, a marker that normally appears soon after denervation, despite evidence that TSCs and SCs in these mice are fully capable of producing P75. These observations suggest that if denervated SOD1 NMJs possess TSCs and preterminal SCs, then these cells behave abnormally after denervation. An alternative possibility is that SOD1 TSCs and preterminal SCs may be absent after denervation. In either case, these observations suggest that distal SCs in SOD1 muscles react abnormally in response to denervation.

In the present study, we examined the response of SOD1 TSCs and SCs to experimental denervation. Results show that these cells lose SC-specific labeling soon after denervation and do not label for P75. In addition, large cells are found near endplate regions soon after denervation which immunolabel for P75, S100 and activated caspase suggesting that SOD1 SC and TSC may become displaced after denervation and experience cell death. These results are considered in the context of the important roles normally played by SCs and TSCs in mediating reinnervation of muscle.

METHODS

Animals

In these experiments, three different transgenic mouse strains of either gender were used, each on a congenic C57BL6/J background to avoid genetic modifier effects of background strain on disease expression (Heiman-Patterson et al., 2011). Most work was conducted using mice which overexpress a transgene that carries the G93A mutation of human SOD1 protein (Gurney et al., 1994). Hereafter, these mice (B6.Cg-Tg(SOD1-G93A)1Gur/J) are referred to as B6.SOD1 mice. In some experiments, mice were used that express the human transgene for the G85R SOD1 mutation (B6.Cg-Tg(SOD1*G85R)148Dwc/J, hereafter $SOD1^{G85R}$). For controls, we used either C57BL6/J (hereafter WT) or transgenic mice that overexpress the wild-type human SOD1 protein (B6.Cg-Tg(SOD1)2Gur/J, hereafter $SOD1^{WT}$ (Gurney et al., 1994). All mice were bred at Emory University or acquired from The Jackson Laboratory (www.jax.org, Bar Harbor, ME). All experiments were carried out in accordance with the Institutional Animal Care and Use Committees of Emory University.

Surgery

Surgeries were performed under general anesthesia (ketamine 95 mg/kg, xylazine 5 mg/kg). Denervation of hindlimb muscles was accomplished by crush of the sciatic nerve. The sciatic nerve was exposed and crushed at a point located 2 mm rostral to the emergence of the common peroneal nerve. Sciatic crush was accomplished using a fine watchmaker's forceps with pressure applied for 10 sec. This caused the nerve to appear translucent at the crush site. Afterwards, fasciae and skin incisions were closed using 6-0 monofilament suture. No additional steps were taken to inhibit reinnervation. The animals were then returned to their cages for recovery. Food and water were administered ad lib following recovery and animals were allowed to move freely in their cages. Sciatic crush denervation was performed in B6.SOD1 and WT mice at P30 and at P60. Denervation was also performed in $SOD1^{WT}$ mice aged P60, and in $SOD1^{G85R}$ mice but at a later age as described in Results. At 10 and/or 14 days after denervation, reinnervation was studied in B6.SOD1, WT, $SOD1^{WT}$ and at 10 days in $SOD1^{G85R}$ mice.

Immunolabeling

Under general anesthesia, the medial gastrocnemius (MG) and soleus muscles from sciatic crush and un-crushed, contralateral control sides were recovered after delays ranging from 16 hrs to 14 days and prepared for immunolabeling. Muscles were placed into 4% paraformaldehyde for 1 hr. Muscles were washed in a 0.1 M phosphate buffered solution (PBS) and incubated at 4°C overnight in PBS containing 20% sucrose for cryoprotection. Sections (50 μm thickness) were obtained using a Cyrostat (Leica). Motor endplate acetylcholine receptors (AChRs) were labeled with either Alexa 488 or Alexa 649 conjugated α-bungarotoxin (Molecular Probes). Axons were labeled with a mouse monoclonal antibody against the phosphorylated heavy fragment of neurofilament protein (SMI31, 1:400, Sternberger Monoclonal). Motor terminal were labeled for synaptic vesicles (SV2, 1:20, Developmental Studies Hybridoma Bank). This labeling was visualized using AMCA-conjugated secondary antibody (1:100, Jackson Immunoresearch Laboratories). Schwann cells (SCs) were labeled with a rabbit polyclonal antibody against the Ca^{2+}-

binding protein S100B (S100, 1:100, Dako) and visualized using a rhodamine-conjugated secondary antibody (1:100, Jackson Immunoresearch Laboratories). In addition to S100 labeling, SCs in some sections were also labeled with a goat polyclonal antibody against the low affinity nerve growth factor receptor p75 (NGFR p75, 1:50, Santa Cruz SC-6188) and visualized using a fluorescein-conjugated secondary antibody (1:100, Jackson Immunoresearch Laboratories). Some sections taken from muscles 16, 24 and 48 hours after denervation were labeled for calpain-mediated amino terminal fodrin fragment (FBDP, 1:150, (Bahr et al., 1995)) as a marker for SC necrosis (Hill et al., 2007) or for activated caspase-3 (BD Pharmigen, 1:100) as a marker for apoptosis (Delaney et al., 1999; Hill et al., 2007). Positive labeling for activated caspase-3 has been shown to appear in SCs under conditions that also produce positive TUNEL labeling (Parkinson et al., 2001). Antibody labeling for caspase-3 was visualized using a rhodamine-conjugated secondary antibody (1:100, Jackson Immunoresearch Laboratories). SCs in these sections were also labeled with a mouse monoclonal antibody against S100B (Anti S100, 1:100, Millipore) and visualized with a fluorescein-conjugated secondary antibody(1:100, Jackson Immunoresearch Laboratories). Where noted, DAPI staining was used to identify SC or TSC cell body nuclei. This staining was performed as per manufacturer's instructions using slide mounting media (Vectashield) which included DAPI. Macrophages were labeled with a rat monoclonal against the 160KD glycoprotein F4/80 (F4/80, 1:20, AbD Serotec MCA497) and visualized using a fluorescein-conjugated secondary antibody (1:100, Jackson Immunoresearch Laboratories).

Electron Microscopy

A number of NMJs were examined using an electron microscope 7d following sciatic crush denervation of a P45 B6.SOD1 animal. Following tissue recovery, an MG muscle was fixed with 4% paraformaldehyde in 0.1 M phosphate buffer (pH 7.4) overnight before washing 2x with the same buffer. NMJs were then labeled with rhodamine-conjugated bungarotoxin and then visualized under a fluorescence microscope. Areas of NMJ clusters were dissected out and placed in Eppendorf tubes to continue fixation in 2.5% glutaraldehyde in 0.1 M cacodylate buffer (pH 7.4) overnight at 4C. Muscle specimens were then washed and postfixed in 1% osmium tetroxide with 1.5% potassium ferrocyanide in the same buffer for one hour. Muscle specimens were subsequently rinsed 2x with de-ionized water and dehydrated through an ethanol series ending with three exchanges of 100% absolute ethanol. Specimens were then infiltrated with a mixture of propylene oxide and Eponate 12 resin (Ted Pella, Inc., Redding, CA) followed by 100% Eponate 12 resin. Finally, tissue was embedded in Beem capsules and placed in a 60 °C oven for 2 days. Following resin polymerization, hardened resin blocks were thin-sectioned at 70 nm. Sections were then picked up with 200 mesh copper grids, stained with 5% aqueous uranyl acetate and 2% lead citrate, and viewed on a JEOL JEM-1400 transmission electron microscope (Tokyo, Japan) equipped with a Gatan BioScan CCD camera (Gatan, Inc., Pleasanton, CA)

Imaging

Z-axis stacks of images of immunolabeled NMJs were obtained at sequential focal planes (1.0 μm separation) using an upright microscope equipped with a motorized stage (Leica). Stacks were deconvolved using a commercially available inverse filter algorithm

(ImagePro). In some cases, stacks of confocal images were obtained. Muscles from the contralateral (uncrushed sciatic) side provided additional control data.

Analysis

Images of NMJs were analyzed at high magnification (100x) to determine the extent to which presynaptic SMI+SV2 labeling overlaid postsynaptic labeling for AChRs in superimposed images. SMI+SV2 labeling was used to assign the following categories of endplate innervation; endplates that exhibited a complete absence of SMI+SV2 labeling were considered to be denervated; endplates that showed SMI+SV2 labeling present in all ACHR-rich endplate arms or branches were considered to be innervated; endplates that showed SMI+SV2 labeling present in some but not all ACHR-rich arms or branches were considered to be partially innervated. For analysis, randomly selected fields of NMJs were first located at low magnification. Then, at high magnification all the NMJs in each field were categorized as described above. The extent of endplate S100 coverage was also assessed at 100x magnification and assigned into 3 categories (full, partial, absent). Additional analyses to assess colabeling for P75, S100 and DAPI labeling at 100x magnification were performed as described in Results. Unless noted otherwise, all NMJ measurements were sampled from 80 NMJs per muscle, and only one MG-soleus pair from the same side was sampled per animal.

TSC cell bodies were identified by S100 and DAPI nuclear colabeling (Love and Thompson, 1998). Multiple DAPI-labeled nuclei are located in the vicinity of the NMJ (see Fig 1). To identify TSC cell bodies, multiple focal planes were viewed using a 100x, oil-immersion objective with a variable aperture used to minimize depth of focus. At each focal plane, fluorescence filters were manually switched while viewing images on a video monitor to ensure that S100 and DAPI labeling were located in identical focal planes. In most cases, these steps were sufficient to either identify TSC cell bodies or to exclude their presence. In more difficult cases, full image stacks of DAPI and S100 labeling were taken to enable finer scrutiny of labeling placement.

Statistics

Two-way contingency tables were used to determine effects of genotype (B6.SOD1 v WT), age or treatment on frequency distributions of categorical variable means describing innervation status (SMI-SV2 labeling), NMJ S100 and P75 labeling coverage, and S100-P75 colabeling status. For comparing average values, nested analysis of variance was used. Tukey's honestly significant difference post-hoc test was used to test the significance of differences between WT, contralateral control and B6.SOD1 average values. All analysis was performed using commercially available software (Systat Inc). Mean values are presented ± 1 SEM.

RESULTS

Immediately after birth, TSCs do not survive denervation but this behavior normally disappears by P30 (Trachtenberg and Thompson, 1996; Hayworth et al., 2006). TSC structural abnormalities are, however, present at P30 in B6.SOD1 muscles (Carrasco et al.,

2016), so we first examined the response of P30 B6.SOD1 TSCS to denervation 4d after sciatic crush. At both WT and SOD1 MG and soleus NMJs, 100% denervation was found, as judged by the complete absence of labeling for axons and synaptic vesicles. S100 labeling was decreased at both WT and B6.SOD1 NMJs, but total absence of labeling was found only at B6.SOD1 NMJs. The mean percentage of fully-covered B6.SOD1 NMJs decreased from 100% at control NMJs to negligible fractions in both MG and soleus muscles, and a considerable percentage of NMJs (mean > 60%) lacked S100 labeling. The post-denervation changes in the distributions of average coverage status for B6.SOD1 soleus and MG NMJs were both significant (Fig 1B,C; Pearson chi square, $P < 0.01$). Figure 1A illustrates an example of a NMJ field from a B6.SOD1 MG muscle in which all NMJs lack S100 labeling. Figure 1A also demonstrates that post-denervation loss of S100 labeling was not restricted to NMJs. S100 labeling also disappeared in preterminal regions and involved SCs normally associated with preterminal motor axon arbors. Nearby, however, brightly-labeling tracks of SCs could still be found (arrows, Fig 1A). Such tracks were routinely observed after denervation and, although difficult to quantify, indicate that only distal SCs and TSCs lose S100 labeling after denervation while more proximal SCs do not. WT MG and soleus NMJs also showed S100 labeling loss after denervation but the changes were statistically significant only in soleus (Fig 1E, F). Unlike B6.SOD1 NMJs, complete loss of S100 labeling was not observed at P30 WT MG NMJs and only rarely at WT soleus NMJs. Moreover, tracks of S100-labeled SCs defining preterminal paths to NMJs persisted intact after denervation in WT soleus and MG muscles (Fig 1D). Similar effects on NMJ S100 labeling were found 24 hrs after denervation at P60 (data not shown). This indicates that loss of labeling occurs quickly after denervation and that subsequent development does not alter the behavior of B6.SOD1 TSCs. These results demonstrate that B6.SOD1 soleus and MG muscles lose S100 labeling at NMJs and in preterminal regions to a far greater extent than age-matched WT muscles.

In order to learn whether the loss of labeling after denervation is specific for S100, P30 muscles were labeled 4d after sciatic crush for both P75 and S100. P75 labeling normally increases in SCs and TSCs after denervation (Taniuchi et al., 1988; Funakoshi et al., 1993). In WT soleus, robust P75-S100 colabeling at NMJs and in preterminal regions was observed after denervation (Fig 2A1,2). Similarly, in B6.SOD1 muscles, P75 labeling was found wherever S100 expression remained 4d after denervation, whereas no P75 labeling was found over NMJs and in preterminal regions that lacked S100 labeling. Examples of these S100-P75 labeling patterns are shown in Fig 2C–D for B6.SOD1 MG. In 3 P30 SOD1 soleus and MG muscles, and in 3 P30 WT soleus muscles, labeling for S100 and P75 was separately classified into full, partial and absent categories for 40 NMJs in each muscle 4d after denervation. Cross-tabulation of these data showed nearly 100% association between the S100-P75 labeling categories for each tested muscle (Pearson chi-square, $p < 0.01$ in each muscle); in only 3 of 360 comparisons did P75 and S100 labeling categories fail to correspond.

The loss of S100 and P75 labeling after denervation is not due to loss of B6.SOD1 muscle activity. We showed previously that 4d of botulinum toxin (BTOX) paralysis produced no change in either innervation or S100 coverage in P60 B6.SOD1 MG muscles (Carrasco et al., 2016). In the present study, these results were also observed 4d after BOTX paralysis of

P30 B6.SOD1 MG muscles (data not shown). In addition, P75 labeling of P30 B6.SOD1 TSCs and SCs was observed after BTOX paralysis as observed by others in WT muscles (Hassan et al., 1994), and P75 labeling was only found where S100 expression was also present (data not shown). This provides additional evidence that B6.SOD1 TSCs and SCs which are able to express S100 immunoreactivity are also able to express P75 and helps exclude that the absence of P75 labeling at denervated P30 or P60 B6.SOD1 NMJs is explained by an inability of B6.SOD1 TSCs to express P75.

Overall, these results demonstrate that both P75 and S100 labeling are lost after denervation in B6.SOD1 muscles. Moreover, the results show that P75 labeling is absent at B6.SOD1 NMJs where S100 labeling is also absent. In this respect, B6.SOD1 NMJs which completely lose S100 labeling after experimental denervation are identical to B6.SOD1 NMJs that have been denervated by the disease process (Carrasco et al., 2016). These results indicate that, unlike WT NMJs, the majority of B6.SOD1 TSCs and preterminal SCs either completely lose the ability to express both S100 and P75 after denervation or the cells themselves are absent from both NMJs and preterminal regions.

TSC cell bodies

Counts of TSC cell bodies identified by S100-DAPI colabeling showed that denervation at P30 did not change average TSC cell body counts at either WT soleus or MG NMJs (Fig 3A, B, $p > 0.05$, nested ANOVA, $N = 4$ muscles in each group). Identical results were obtained 24hrs after denervation at P60 (data not shown).

A similar analysis of P30 B6.SOD1 NMJs was not possible because the majority (mean ~60%) of B6.SOD1 soleus and MG NMJs lack S100 labeling after denervation (see Fig 1B, C). Thus, TSC nuclei cannot be identified by S100-DAPI colabeling at these NMJs. Examination of the remaining 40% of NMJs that possessed partial S100 coverage showed that TSC cell bodies could still be identified. Most of these partially-covered TSCs in the MG had identifiable TSCs (Fig 3C). This observation could indicate that MG NMJs initially covered only by the processes of SCs (~ 50%, (Carrasco et al., 2016)) lose S100 labeling faster than those covered by TSCs. However, most control P30 B6.SOD1 soleus NMJs possess TSCs, and the overall similarity of shape between control and post-denervation distributions of TSC counts (Fig 3D) suggests that loss of S100 labeling bears little relation to TSC number. A comparison of TSC cell number at full and partially S100 covered NMJs was made between control and denervated P60 B6.SOD1 soleus NMJs. The results showed that TSC cell number per NMJ was significantly lower than control after denervation (control, 1.21 ± 0.04; denervated, 0.81 ± 0.04; $p = 0.02$, nested ANOVA, $N = 4$ muscles in each group). These results indicate that some B6.SOD1 soleus TSCs are lost by 24 hrs after denervation at P60. We attempted to locate possible examples of TSCs vacating B6.SOD1 soleus NMJs 24 hrs after denervation, and several were found 24 hrs after denervation in which TSC cell bodies appeared to have moved off the NMJ but remained attached to processes overlying endplate ACHR labeling (Fig 4).

SCs label for activated caspase after denervation

After sciatic crush denervation of B6.SOD1 muscles at P30 and P60, large S100+ cells were observed that exhibited discontinuities of the cell perimeter and small, brightly-labeled S100+ fragments within the cell. These cells featured large single nuclei and were found in endplate and preterminal regions but never directly overlying endplates. Examples of these features from P30 and P60 muscles are shown in Fig 5A–C. Labeling for P75 showed that virtually 100% of more than 100 S100+ cells like that shown in Figs 5C and studied 72 hrs after sciatic crush at P60 colabeled for P75 in 2 B6.SOD1 MG muscles (Fig 5D1–2). Similar results were obtained with more limited sampling from 2 P30 MG muscles examined 4d after sciatic crush (Fig 5E). Since some macrophages reportedly can express S100 (Donato et al., 2013), muscle sections were labeled for F4/80 which is commonly used as a marker for macrophages (Murray and Wynn, 2011). In sections of B6.SOD1 MG muscle studied 72 hrs after sciatic crush denervation, 50 S100+ cells with the appearance shown in Fig 5B–E were examined for colabeling with F4/80 and no instances of colabeling were found. An example of this independent labeling is shown in Fig 5F. Based on these observations, we conclude that the S100+ cells shown in Fig 5A–E are SCs that are likely to have become displaced from their original locations after denervation.

Based on their appearance, we considered the possibility that these SCs could be undergoing cell death. In order to test this idea, immunolabeling for activated caspase-3 was used as a marker for apoptosis. This marker has been used to detect SC apoptosis in vitro and in vivo (Delaney et al., 1999; Parkinson et al., 2001; Hill et al., 2007). Results from 9 P60 B6.SOD1 MG muscles studied 16 or 24 hrs after sciatic crush showed that S100+ cells such as in Fig 5A–E labeled intensely for activated caspase-3, as shown in Fig 5G for a pair of S100+ cells observed 16 hrs after P60 denervation. In other cases, a wide range of S100/caspase-3 colabeling status could be observed among adjacent cells suggesting an asynchronous appearance of activated caspase labeling. An example of this range is shown in Fig 5H1–2 where cells labeling only for S100 are located nearby cells labeling primarily for caspase and other cells which show more graded colabeling. In this case, S100+/caspase-3+ cells were located in lines suggesting that these SCs had been associated with preterminal axons. In all MG muscles examined and in additional samples from soleus muscles (N = 2), no cases were observed 16–72 hrs after denervation in which activated caspase-3+ cells (with or without S100 colabeling) were found to directly overlie endplates (where TSCs are normally located) but rather as individual cells displaced from nearby endplates (FIg 5A, C) or arranged in lines.

In order to quantify the overall level of apoptosis in B6.SOD1 MG muscles, cells labeling for activated caspase-3 were counted in 50 μm sections taken every 150 μm from MG muscles after denervation. The counts were compared between B6.SOD1 and WT muscles. The results showed that a significant number of caspase+ cells were present in B6.SOD1 MG muscles by 16 hrs after denervation and that this number almost doubled by 24 hrs (Fig 5I). Interestingly, as also reported for distal nerve after sciatic crush (Ferri and Bisby, 1999), a few S100+/caspase+ cells were observed in WT MG muscles 24 hrs after denervation.

We also used immunolabeling for fodrin breakdown product. This antibody (FDBP) is considered to be a marker for necrosis in SCs (Hill et al., 2007) and labels only calpain-

mediated breakdown products of the cytoskeletal protein spectrin (Bahr et al., 1995). FDBP labeling was performed in MG and soleus muscles from 4 B6.SOD1 mice at 16, 24 and 48 hrs after sciatic crush at P60. We were unable to find convincing evidence of any FBDP labeling at NMJs or in preterminal regions at any time point in cells that also labeled for S100 (data not shown). Overall, our evidence indicates that apoptosis of B6.SOD1 TSCs and preterminal SCs begins soon after sciatic crush denervation.

Electron microscopy

The above results suggest that preterminal SCs and TSCs are lost at B6.SOD1 NMJs after denervation. In order to verify these immunolabeling results, B6.SOD1 MG NMJs were examined using electron microscopy. The sciatic nerve of a P45 B6.SOD1 mouse was crushed and the MG muscle recovered 7d later. P45 was selected to lie between P30 and P60, while a 7d denervation period was selected because of evidence that loss of S100 labeling increases between 1d and 10d after denervation at P60 (see below). Inspection of 4 endplates showed that all lacked identifiable structures or cells located immediately above secondary folds. An example is shown in Fig 6 which illustrates the entire longitudinal extent of a B6.SOD1 MG endplate (Fig 6A). Because of denervation 7d earlier, no axon or motor terminal can be seen. No identifiable structures that resemble TSCs or TSC processes lie immediately over the endplate. Following denervation, WT TSCs remain identifiable and retain intimate coverage of a majority (~ 70%) of endplate secondary folds for at least 10d after denervation as shown by others (Kang et al., 2014). As shown in Fig 6, however, the areas immediately over the B6.SOD1 MG endplate secondary folds are instead occupied primarily by debris and collagen fibrills. A long, ribbon-like structure may also be seen that extends the length of the endplate (indicated by red arrows in B and C). Although the identity of this structure is unknown, it does not appear to have an intimate relationship with endplate secondary folds. Overall, the appearance of these endplates resembles the ultrastructural appearance of denervated normal endplates where reinnervation has been prevented for weeks (Miledi and Slater, 1968). Under these conditions, TSCs also vacate endplates. These observations further support the indications provided by immunolabeling studies that TSCs are lost from B6.SOD1 NMJs soon after denervation.

Reinnervation of B6.SOD1 NMJs

Innervation and S100 labeling were examined 10d and 14d after sciatic crush performed at P60. By 10d, neither B6.SOD1 nor WT MG NMJs were completely reinnervated; the distributions of innervation categories were each significantly different from distributions of contralateral, untreated muscles (Pearson chi-square, $p < 0.01$, Fig 7C, D). Moreover, the SOD1 and WT sciatic crush side distributions differed significantly from each other indicating that reinnervation of WT NMJs was more advanced than B6.SOD1 NMJs at 10d despite identical placement of sciatic crush in each case. At 10d, all WT NMJs were fully covered by S100 independent of innervation status (Fig 7A, D). In contrast, all denervated B6.SOD1 NMJs lacked S100 labeling while fully or partially reinnervated NMJs were fully or partially covered by S100 labeling, respectively (Fig 7B, C). Since denervated NMJs which lack S100 labeling constitute about 95% of the sample, it appears that almost all B6.SOD1 MG NMJs eventually lose S100 labeling in the days following denervation. An absence of S100 labeling was also observed in preterminal regions of B6.SOD1 MG

muscles which in WT MG muscles featured robust labeling of SCs associated with preterminal axons (cf Fig 7A, B). In some sections of B6.SOD1 muscles, however, bundles of S100-labeled SCs (Fig 7G1, white outline) could be found that appeared to be extending into endplate regions that were completely devoid of axons, S100-labeled SCs or processes that normally lead to and cover endplates. Colabeling these S100-labled bundles for NF revealed the presence of axons regenerating in close association with SC processes but extending no further than the limits of the processes (Fig. 7G2). These observations indicate that 10 days after sciatic crush, B6.SOD1 motor axons regenerate in close association with SC processes extending into endplate regions that appear to be devoid of SCs or SC processes.

In 2 B6.SOD1 MG muscles studied 10 days after sciatic crush, P75 colabeling was examined at endplates and in preterminal areas. The results showed 100% P75 and S100 colabeling; cross-tabulation analysis of the presence or absence of P75 and S100 colabeling at or near endplates was significant in each examined muscle (Pearson Chi-square, $p < 0.01$). An example of this colabeling near a denervated B6.SOD1 MG endplate 10 days after sciatic crush is shown in Fig 7F. As was the case for P30 denervation, these results demonstrate that where S100 labeling is present or absent 10 days after denervation of the SOD1 MG muscle, P75 labeling is also present or absent.

Reinnervation status and endplate S100 coverage were also examined 14 days after sciatic crush in MG muscles from B6.SOD1, WT controls and $SOD1^{WT}$ mice. The results showed that WT and $SOD1^{WT}$ MG muscles were almost completely reinnervated and that all NMJs were completely covered by S100 labeling (Fig 7I, J). Reinnervation of B6.SOD1 MG muscles had progressed relative to 10 day post-crush, but MG muscles studied 14 days after sciatic crush remained considerably less reinnervated than WT and $SOD1^{WT}$ muscles, and denervated endplates still lacked overlying S100 labeling. The fact that $SOD1^{WT}$ and WT MG NMJs were reinnervated to a similar extent after sciatic crush and show complete S100 NMJ coverage indicates that simple overexpression of SOD1 protein does not underlie the reinnervation delays and S100 labeling loss observed in B6.SOD1 muscles after denervation. These results provide further evidence that reinnervation of B6.SOD1 MG muscle proceeds more slowly than in WT MG muscle.

Post-denervation loss of NMJ S100 is not specific for G93A mutation

To determine if the effects of denervation are specific for the G93A SOD1 mutation, sciatic crush denervation was studied in mice that express the G85R SOD1 mutation. The disease time course in $SOD1^{G85R}$ mice is considerably longer (8–10 mo overt onset) than in B6.SOD1 mice (~4.5 month overt onset, Wooley et al., 2005). In order to achieve comparable timing, sciatic crush in $SOD1^{G85R}$ mice was performed at 160 days instead of 60 days as in B6.SOD1 mice so that experimental denervation was performed at about mid-lifespan in both. At this age, all $SOD1^{G85R}$ NMJs are innervated and fully covered by S100 labeling but many show the same type of TSC structural abnormalities observed by P30 in B6.SOD1 mice (Carrasco et al., 2016). Innervation status and endplate S100 coverage in MG muscles of $SOD1^{G85R}$ mice were examined 10 days after sciatic crush, and all denervated endplates in $SOD1^{G85R}$ MG muscles were found to lack S100 labeling (Fig 7E).

The response to denervation was not, however, identical to that of B6.SOD1 NMJs since SOD1^{G85R} MG muscles showed relatively more extensive reinnervation 10 days after denervation. Nevertheless, these data demonstrate that post-denervation loss of endplate S100 labeling is not specific for the G93A SOD1 mutation. Since SOD1^{G85R} mice express the transgene for the G85R SOD1 mutation at much lower levels than the G93A transgene is expressed in B6.SOD1 mice (≤ 1x vs ~ 20x endogenous levels, (Gurney et al., 1994; Bruijn et al., 1997)), these results provide further evidence that overexpression of the SOD1 protein underlies the response of B6.SOD1 SCs and TSCs to denervation.

DISCUSSION

The purpose of this study was to learn how distal B6.SOD1 SCs and TSCs react to denervation. The motivation for this study derived from observations of NMJs in B6.SOD1 control mice that had been denervated by the disease process and appeared to lack TSC and SC S100 labeling in preterminal areas (Carrasco et al., 2016). The results of this study demonstrate that TSCs and distal SCs of B6.SOD1 muscles react abnormally to experimental denervation. At P30 and P60, S100 labeling is lost at B6.SOD1 NMJs quickly and to a far greater extent than at WT NMJs after denervation (Fig 1). By 10d after P60 denervation, B6.SOD1 NMJs have lost all S100 labeling (Fig 7). In addition, S100 labeling is lost in preterminal regions in B6.SOD1 but not WT muscles after denervation (Fig 1, 7). The loss of labeling in B6.SOD1 muscles is not specific for S100 since P75 labeling is also lost after denervation (Fig 2). This loss occurs despite the facts that P75 labeling is normally increased after denervation in WT muscles and that B6.SOD1 SCs and TSCs are fully capable of upregulating P75 labeling as seen after BOTX treatment. In addition, cells that label for activated caspase 3, P75 and S100 are found to a far greater extent in B6.SOD1 muscles after denervation (Fig 5) and seem likely to be displaced TSCs or SCs.

The simplest explanation of these observations is that, unlike the case in WT muscles, many distal B6.SOD1 SCs and TSCs become displaced and experience cell death after denervation. EM evidence supports this conclusion by showing an absence of cells opposing B6.SOD1 endplates 7d after denervation (Fig 6). Loss of distal SCs and TSCs can also help explain patterns observed during reinnervation of B6.SOD1 muscle. B6.SOD1 axons appear to regenerate in the company of SCs rather than along SC pathways into endplates bands which lack S100 labeling altogether (Fig 7G). This pattern of axonal regeneration suggests that reinnervation involves replacement of distal SCs by more proximal SCs that survive denervation and migrate with regenerating axons. The need to replace the distal-most population of SCs helps explain why reinnervation of B6.SOD1 muscle occurs more slowly than WT (Fig 7), as also noted by others (Pun et al., 2006; Lobsiger et al., 2009). This mode of reinnervation fits with evidence that axonal regeneration into regions of muscle that lack pre-existing SCs is limited by the rate of SC extension (Son et al., 1996). Evidence also showed that 10d after denervation, SOD1^{G85R} MG muscles were reinnervated to a greater extent than B6.SOD1 MG muscles (Fig 7). SOD1^{G85R} MG control sides were almost completely innervated while B6.SOD1 MG control muscles were not. Thus, the differences in reinnervation may reflect an inexact matching of disease progression between these groups. Whether this is also associated with less loss of preterminal SCs in SOD1^{G85R} MG muscles after denervation remains to be determined. Following denervation, SCs normally

participate in clearing axonal debris and myelin. Thus, altered clearance of distal axonal debris and myelin because of the loss of distal B6.SOD1 SCs might contribute to slowed reinnervation of B6.SOD1 muscle. However, myelin clearance is also mediated by macrophages (Stoll et al., 1989; Hirata and Kawabuchi, 2002), and these cells are clearly present after denervation in B6.SOD1 muscle (Fig 5F). Moreover, we do not yet know whether B6.SOD1 axons regenerate through original endoneurial tubes where uncleared axonal debris can impede regeneration (Kang and Lichtman, 2013). It thus remains possible that endoneurial tubes are recreated and unlikely to be blocked by axonal debris.

An important issue to consider is why B6.SOD1 SCs and TSCs react abnormally to denervation. Our results enable us to exclude several factors. Thus, the genotype and expression levels of the SOD1 mutation do not appear to be contributing factors. Support for this is evidence from mice that express the G85R SOD1 mutation at less than 1x normal SOD1 levels and possess NMJs which also lose S100 after denervation, with all denervated NMJs exhibiting an absence of S100 labeling (Fig 7). In addition, mice that overexpress the unmutated WT SOD1 gene appear to reinnervate as efficiently as WT mice after denervation (Fig 7). The post-denervation behavior of B6.SOD1 TSCs and SCs does not depend on loss of activity since BOTX paralysis does not affect S100 labeling at B6.SOD1 NMJs (Carrasco et al., 2016). This suggests that B6.SOD1 distal SCs and TSCs respond instead to loss of physical contact with axons or, possibly, to some toxicity acquired as a result of axon or motor terminal degeneration. Phagocytosis of the products of axonal degeneration (Miledi and Slater, 1970; Manolov, 1974) could be a mechanism by which SCs obtain such material. Our results show, however, that not all SCs that are exposed to degenerating B6.SOD1 axons die; SCs between the sciatic crush site and the general location of preterminal SCs are also exposed to degenerating B6.SOD1 axons but appear to survive and supply SCs during reinnervation. Any toxic effects of degenerating B6.SOD1 axons would thus reach lethal levels only for distal SCs while being nonexistent or below lethal levels elsewhere. Another factor to consider is that sciatic crush denervation appears to cause loss of all preterminal SCs and TSCs. Thus, any toxic products of axon degeneration need to derive from all B6.SOD1 distal motor axons and terminals independent of the disease status of individual axons.

An alternative but not necessarily exclusive possibility is provided by developmental studies. Apoptosis of preterminal SCs and TSCs occurs following denervation of neonatal (P5) muscle (Trachtenberg and Thompson, 1996; Hayworth et al., 2006). In this case, distal SCs die because they lack an adult phenotype and remain dependent on neuregulin signaling from axons for survival which is lost after axotomy. During subsequent development, autocrine mechanisms emerge that enable SC survival in the absence of axonal contact (Cheng et al., 1998; Meier et al., 1999). Thus, one possibility is that B6.SOD1 distal SCs may be lost after denervation because these developmental steps do not occur and distal SCs remain immature. We recently showed that other TSC abnormalities are present by P30 at B6.SOD1 NMJs. Analysis of control P30 MG muscles showed that while all NMJs were fully innervated, many were not occupied by TSCs but were instead fully covered by the processes of SCs whose cell bodies were located proximally along preterminal axons (Carrasco et al., 2016). All P30 soleus NMJs, by contrast, were fully covered by one or more TSCs. At birth, other studies have shown that many but not all NMJs are similarly not

covered by TSCs, and that eventual TSC coverage occurs after SCs migrate along preterminal axons into NMJs (Love and Thompson, 1998). Thus, the abnormal coverage of some P30 NMJs could arise if SC migration was disrupted during postnatal development. Evidence of possible developmental abnormalities does not necessarily mean that B6.SOD1 distal TSCs/SCs are lost after denervation because they have not matured normally. Moreover, the post-denervation response appears to involve all distal SCs and TSCs; no apparent differences in the response between B6.SOD1 MG and soleus muscles were observed. The significance of this difference is not clear and could mean that different underlying mechanisms are involved. However, taken together, the evidence appears to establish that significant developmental abnormalities exist in B6.SOD1 muscles that could include lack of maturity in distal SCs.

It remains to be determined whether the abnormal response of B6.SOD1 SCs to denervation depends on mutant SOD1 protein expression in SCs/TSCs, motor axons or all cell types. Limited evidence suggests that mutant expression in axons and motor terminals may be sufficient to enable abnormal NMJ coverage by SCs. NMJs that lack TSCs and are covered by the processes of remotely-located SCs have been observed in SOD1 mice in which expression of mutant SOD1 protein in SCs is inhibited (Lobsiger et al., 2009). Whether distal SCs respond abnormally and are lost after denervation under these conditions is not yet known.

Consequences

After partial denervation, normal TSCs at denervated NMJs extend processes that grow and contact TSC processes extending from nearby innervated endplates. The interaction creates a “bridge” over which sprouts from intact motor terminals are induced to grow and reinnervate denervated endplates (Son and Thompson, 1995a, b). This process is thought to help compensate for asynchronous loss of motor unit function in motor neuron disease (Stalberg, 1982). Because distal B6.SOD1 SCs and TSCs are lost following denervation, our results suggest that any motor terminal sprouting that may occur from innervated endplates is unlikely to provide successful compensatory reinnervation in B6.SOD1 mice. Moreover. many innervated P30 SOD1 MG endplates are covered by processes from SCs from remotely-located cell bodies and it is unclear whether extra processes needed to effect terminal sprouting can be produced at such endplates. Terminal sprouts have been observed in SOD1 mice (Frey et al., 2000; Pun et al., 2006), but other studies have reported that terminal sprouting is rare in $SOD1^{G93A}$ muscles (Schaefer et al., 2005; Gould et al., 2006). Under conditions of defective terminal sprouting, compensatory reinnervation would be limited to nodal sprouting in which sprouts emerge from more proximal nodes of Ranvier of intact axons (Slack et al., 1979; Hopkins and Slack, 1981). Reinnervation by this mechanism may be further slowed because of the need to replace SCs along the regenerating paths to NMJs, as observed after sciatic denervation (Fig 7G). A related question is whether truly effective compensatory reinnervation occurs at all in muscle of $SOD1^{G93A}$ mice. Limited available evidence suggests that this may not be the case; using indirect estimates, Hegedus et (2007) found that average motor unit size in hindlimb muscles does not increase with disease progression as would be expected if surviving motor neurons expanded their functional motor unit size by successfully reinnervating denervated muscle fibers.

It is not yet possible to specify whether the abnormalities of $SOD1^{G93A}$ SCs and TSCs reported here are the result of dysfunctional motor neurons, SCs or both. Moreover, if $SOD1^{G93A}$ TSCs are indeed immature, questions arise about whether the underlying motor terminals are stable. Normal TSCs detect activity in motor terminals (Rochon et al., 2001; Todd et al., 2010) and may have an important trophic relationship with motor terminals as suggested by observations that eliminating TSCs is followed by motor terminal degeneration (Koirala et al., 2003; Reddy et al., 2003). It may thus be that disruptions of a relationship like this might contribute to motor terminal degeneration in motor neuron disease.

Acknowledgments

This work was supported by NIH grants NS31621 and NS074231. The authors wish to thank Ms Hong Yi for electron microscopy. The Robert P. Apkarian Integrated Electron Microscopy Core of Emory University is supported by NIH grant S10RR025679.

References

Arbour D, Tremblay E, Martineau E, Julien JP, Robitaille R. Early and persistent abnormal decoding by glial cells at the neuromuscular junction in an ALS model. J Neurosci. 2015; 35:688–706. [PubMed: 25589763]

Bahr BA, Tiriveedhi S, Park GY, Lynch G. Induction of calpain-mediated spectrin fragments by pathogenic treatments in long-term hippocampal slices. J Pharmacol Exp Ther. 1995; 273:902–908. [PubMed: 7538583]

Balice-Gordon RJ, Smith DB, Goldman J, Cork LC, Shirley A, Cope TC, Pinter MJ. Functional motor unit failure precedes neuromuscular degeneration in canine motor neuron disease. Ann Neurol. 2000; 47:596–605. [PubMed: 10805330]

Bruijn LI, Becher MW, Lee MK, Anderson KL, Jenkins NA, Copeland NG, Sisodia SS, Rothstein JD, Borchelt DR, Price DL, Cleveland DW. ALS-linked SOD1 mutant G85R mediates damage to astrocytes and promotes rapidly progressive disease with SOD1-containing inclusions. Neuron. 1997; 18:327–338. [PubMed: 9052802]

Burkholder TJ, Fingado B, Baron S, Lieber RL. Relationship between muscle fiber types and sizes and muscle architectural properties in the mouse hindlimb. J Morphol. 1994; 221:177–190. [PubMed: 7932768]

Carrasco DI, Seburn KL, Pinter MJ. Altered terminal Schwann cell morphology precedes denervation in SOD1 mice. Exp Neurol. 2016; 275(Pt 1):172–181. [PubMed: 26416261]

Cheng L, Esch FS, Marchionni MA, Mudge AW. Control of Schwann cell survival and proliferation: autocrine factors and neuregulins. Mol Cell Neurosci. 1998; 12:141–156. [PubMed: 9790735]

Darabid H, Arbour D, Robitaille R. Glial cells decipher synaptic competition at the mammalian neuromuscular junction. J Neurosci. 2013; 33:1297–1313. [PubMed: 23345206]

Delaney CL, Cheng HL, Feldman EL. Insulin-like growth factor-I prevents caspase-mediated apoptosis in Schwann cells. J Neurobiol. 1999; 41:540–548. [PubMed: 10590177]

Donato R, Cannon BR, Sorci G, Riuzzi F, Hsu K, Weber DJ, Geczy CL. Functions of S100 proteins. Curr Mol Med. 2013; 13:24–57. [PubMed: 22834835]

Ferri CC, Bisby MA. Improved survival of injured sciatic nerve Schwann cells in mice lacking the p75 receptor. Neurosci Lett. 1999; 272:191–194. [PubMed: 10505613]

Fischer LR, Culver DG, Tennant P, Davis AA, Wang M, Castellano-Sanchez A, Khan J, Polak MA, Glass JD. Amyotrophic lateral sclerosis is a distal axonopathy: evidence in mice and man. Exp Neurol. 2004; 185:232–240. [PubMed: 14736504]

Frey D, Schneider C, Xu L, Borg J, Spooren W, Caroni P. Early and selective loss of neuromuscular synapse subtypes with low sprouting competence in motorneuron diseases. J Neurosci. 2000; 20:2534–2542. [PubMed: 10729333]

Funakoshi H, Frisen J, Barbany G, Timmusk T, Zachrisson O, Verge VM, Persson H. Differential expression of mRNAs for neurotrophins and their receptors after axotomy of the sciatic nerve. J Cell Biol. 1993; 123:455–465. [PubMed: 8408225]

Gould TW, Buss RR, Vinsant S, Prevette D, Sun W, Knudson CM, Milligan CE, Oppenheim RW. Complete dissociation of motor neuron death from motor dysfunction by Bax deletion in a mouse model of ALS. J Neurosci. 2006; 26:8774–8786. [PubMed: 16928866]

Gurney ME, Pu H, Chiu AY, Dal Canto MC, Polchow CY, Alexander DD, Caliendo J, Hentati A, Kwon YW, Deng HX, Chen W, Zhai P, Sufit RL, Siddique T. Motor neuron degeneration in mice that express a human Cu,Zn superoxide dismutase mutation. Science. 1994; 264:1772–1775. [PubMed: 8209258]

Hassan SM, Jennekens FG, Veldman H, Oestreicher BA. GAP-43 and p75NGFR immunoreactivity in presynaptic cells following neuromuscular blockade by botulinum toxin in rat. J Neurocytol. 1994; 23:354–363. [PubMed: 8089707]

Hayworth CR, Moody SE, Chodosh LA, Krieg P, Rimer M, Thompson WJ. Induction of neuregulin signaling in mouse schwann cells in vivo mimics responses to denervation. J Neurosci. 2006; 26:6873–6884. [PubMed: 16793894]

Heiman-Patterson TD, Sher RB, Blankenhorn EA, Alexander G, Deitch JS, Kunst CB, Maragakis N, Cox G. Effect of genetic background on phenotype variability in transgenic mouse models of amyotrophic lateral sclerosis: a window of opportunity in the search for genetic modifiers. Amyotroph Lateral Scler. 2011; 12:79–86. [PubMed: 21241159]

Hill CE, Hurtado A, Blits B, Bahr BA, Wood PM, Bartlett Bunge M, Oudega M. Early necrosis and apoptosis of Schwann cells transplanted into the injured rat spinal cord. Eur J Neurosci. 2007; 26:1433–1445. [PubMed: 17880386]

Hirata K, Kawabuchi M. Myelin phagocytosis by macrophages and nonmacrophages during Wallerian degeneration. Microsc Res Tech. 2002; 57:541–547. [PubMed: 12112437]

Hopkins WG, Slack JR. The sequential development of nodal sprouts in mouse muscles in response to nerve degeneration. J Neurocytol. 1981; 10:537–556. [PubMed: 7310464]

Kang H, Lichtman JW. Motor axon regeneration and muscle reinnervation in young adult and aged animals. J Neurosci. 2013; 33:19480–19491. [PubMed: 24336714]

Kang H, Tian L, Mikesh M, Lichtman JW, Thompson WJ. Terminal Schwann cells participate in neuromuscular synapse remodeling during reinnervation following nerve injury. J Neurosci. 2014; 34:6323–6333. [PubMed: 24790203]

Koirala S, Reddy LV, Ko CP. Roles of glial cells in the formation, function, and maintenance of the neuromuscular junction. J Neurocytol. 2003; 32:987–1002. [PubMed: 15034281]

Lobsiger CS, Boillee S, McAlonis-Downes M, Khan AM, Feltri ML, Yamanaka K, Cleveland DW. Schwann cells expressing dismutase active mutant SOD1 unexpectedly slow disease progression in ALS mice. Proc Natl Acad Sci U S A. 2009; 106:4465–4470. [PubMed: 19251638]

Love FM, Thompson WJ. Schwann Cells Proliferate at Rat Neuromuscular Junctions during Development and Regeneration. J Neuroscience. 1998; 18:9376–9385. [PubMed: 9801376]

Manolov S. Initial changes in the neuromuscular synapses of denervated rat diaphragm. Brain Res. 1974; 65:303–316. [PubMed: 4420951]

Meier C, Parmantier E, Brennan A, Mirsky R, Jessen KR. Developing Schwann cells acquire the ability to survive without axons by establishing an autocrine circuit involving insulin-like growth factor, neurotrophin-3, and platelet-derived growth factor-BB. J Neurosci. 1999; 19:3847–3859. [PubMed: 10234017]

Miledi R, Slater CR. Electrophysiology and electron-microscopy of rat neuromuscular junctions after nerve degeneration. Proc R Soc Lond B Biol Sci. 1968; 169:289–306. [PubMed: 4384567]

Miledi R, Slater CR. On the degeneration of rat neuromuscualr junctions after nerve section. J Physiol. 1970; 207:507–528. [PubMed: 5499034]

Murray PJ, Wynn TA. Protective and pathogenic functions of macrophage subsets. Nat Rev Immunol. 2011; 11:723–737. [PubMed: 21997792]

Parkinson DB, Dong Z, Bunting H, Whitfield J, Meier C, Marie H, Mirsky R, Jessen KR. Transforming growth factor beta (TGFbeta) mediates Schwann cell death in vitro and in vivo: examination of c-Jun activation, interactions with survival signals, and the relationship of

TGFbeta-mediated death to Schwann cell differentiation. J Neurosci. 2001; 21:8572–8585. [PubMed: 11606645]

Pun S, Santos AF, Saxena S, Xu L, Caroni P. Selective vulnerability and pruning of phasic motoneuron axons in motoneuron disease alleviated by CNTF. Nat Neurosci. 2006; 9:408–419. [PubMed: 16474388]

Reddy LV, Koirala S, Sugiura Y, Herrera AA, Ko CP. Glial cells maintain synaptic structure and function and promote development of the neuromuscular junction in vivo. Neuron. 2003; 40:563–580. [PubMed: 14642280]

Rochon D, Rousse I, Robitaille R. Synapse-glia interactions at the mammalian neuromuscular junction. J Neurosci. 2001; 21:3819–3829. [PubMed: 11356870]

Sagot Y, Tan SA, Hammang JP, Aebischer P, Kato AC. GDNF Slows Loss of motoneurons but Not Axonal Degeneration or Premature Death of pmn/pmn Mice. J Neurosci. 1996; 16:2335–2341. [PubMed: 8601813]

Schaefer AM, Sanes JR, Lichtman JW. A compensatory subpopulation of motor neurons in a mouse model of amyotrophic lateral sclerosis. J Comp Neurol. 2005; 490:209–219. [PubMed: 16082680]

Slack JR, Hopkins WG, Williams MN. Nerve sheaths and motoneurone collateral sprouting. Nature. 1979

Son YJ, Thompson WJ. Nerve sprouting in muscle is induced and guided by processes extended by Schwann cells. Neuron. 1995a; 14:133–141. [PubMed: 7826631]

Son YJ, Thompson WJ. Schwann cell processes guide regeneration of peripheral axons. Neuron. 1995b; 14:125–132. [PubMed: 7826630]

Son YJ, Trachtenberg JT, Thompson WJ. Schwann cells induce and guide sprouting and reinnervation of neuromuscular junctions. Trends Neurosci. 1996; 19:280–285. [PubMed: 8799973]

Stalberg, E. Electrophysiological studies of reinnervation in ALS. In: Rowland, LP., editor. Human Motor Neuron Diseases. New York: Raven Press; 1982. p. 47-59.

Stoll G, Griffin JW, Li CY, Trapp BD. Wallerian degeneration in the peripheral nervous system: participation of both Schwann cells and macrophages in myelin degradation. J Neurocytol. 1989; 18:671–683. [PubMed: 2614485]

Taniuchi M, Clark HB, Schweitzer JB, Johnson EM Jr. Expression of nerve growth factor receptors by Schwann cells of axotomized peripheral nerves: ultrastructural location, suppression by axonal contact, and binding properties. J Neurosci. 1988; 8:664–681. [PubMed: 2828568]

Todd KJ, Darabid H, Robitaille R. Perisynaptic glia discriminate patterns of motor nerve activity and influence plasticity at the neuromuscular junction. J Neurosci. 2010; 30:11870–11882. [PubMed: 20810906]

Trachtenberg JT, Thompson WJ. Schwann cell apoptosis at developing neuromuscular junctions is regulated by glial growth factor. Nature. 1996; 379:174–177. [PubMed: 8538769]

Wooley CM, Sher RB, Kale A, Frankel WN, Cox GA, Seburn KL. Gait analysis detects early changes in transgenic SOD1(G93A) mice. Muscle Nerve. 2005; 32:43–50. [PubMed: 15880561]

Highlights

- The response of Schwann cells (SCs) to denervation was studied in muscles of SOD1^{G93A} mice
- At P30 or P60, S100 labeling quickly disappeared from SOD1^{G93A} neuromuscular junctions (NMJs) and from preterminal regions of endplate bands.
- These effects did not depend on loss of activity and were not specific for S100 labeling
- Other evidence suggests that distal SCs may be lost after denervation of SOD1^{G93A} muscles
- The abnormal response of SOD1^{G93A} distal SCs to denervation will likely slow or inhibit reinnervation following disease-related denervation

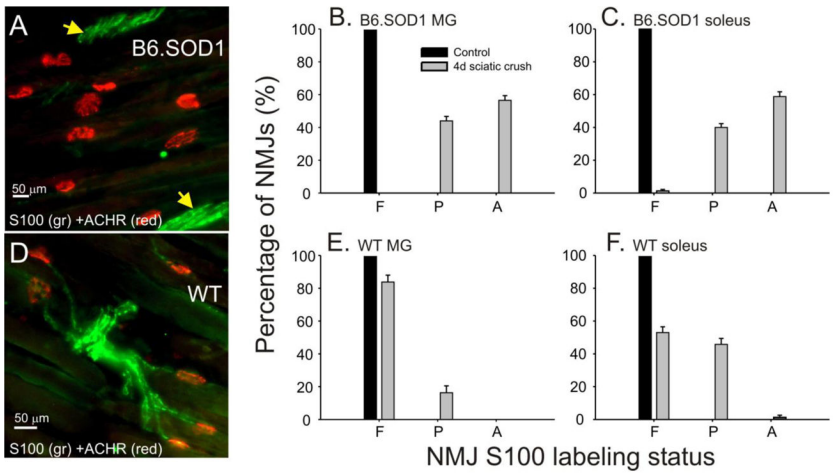

Figure 1.

Loss of S100 labeling at B6.SOD1 NMJs following sciatic crush denervation at P30. A. Field of NMJs from a B6.SOD1 MG muscle 4d after denervation labeled for S100 (green) and acetylcholine receptors (ACHRs, red). Panel demonstrates the absence of S100 labeling over ACHR-labeled endplates and in the immediate preterminal regions whereas S100 labeling of SCs can still be found in more proximal trunks (yellow arrows). B, C. NMJs were viewed at high magnification (100x) and classified into 3 categories based on the extent that each NMJ was covered by S100 labeling. Bar charts show average percentages for categories of NMJ S100 coverage (F, full; P, partial; A, absent) 4d after denervation for P30 B6.SOD1 MG (B, N = 4) and soleus (C, N = 4). Control B6.SOD1 MG and soleus NMJs are fully covered by S100 labeling. After denervation, full S100 coverage disappears and a significant percentage of NMJs show an absence of S100 coverage. Post-denervation changes of S100 coverage distributions were statistically significant (Pearson chi-square, $p < 0.01$). D. Panel shows S100 labeling in an NMJ field from a P30 WT MG muscle 4d after denervation. S100 labeling persisted in preterminal regions and over most NMJs demonstrating continued presence of TSCs and SCs following denervation. E, F. Bar charts show average percentages for categories of NMJ S100 coverage 4d after sciatic crush denervation for P30 WT MG (E, N = 4) and soleus (F, N = 4). For each muscle, some S100 labeling was lost after denervation and the post-denervation changes in the soleus muscle were statistically significant. Unlike B6.SOD1 NMJs, however, only a small fraction of WT soleus NMJs showed an absence of S100 labeling while most WT MG NMJs retained full S100 coverage after denervation.

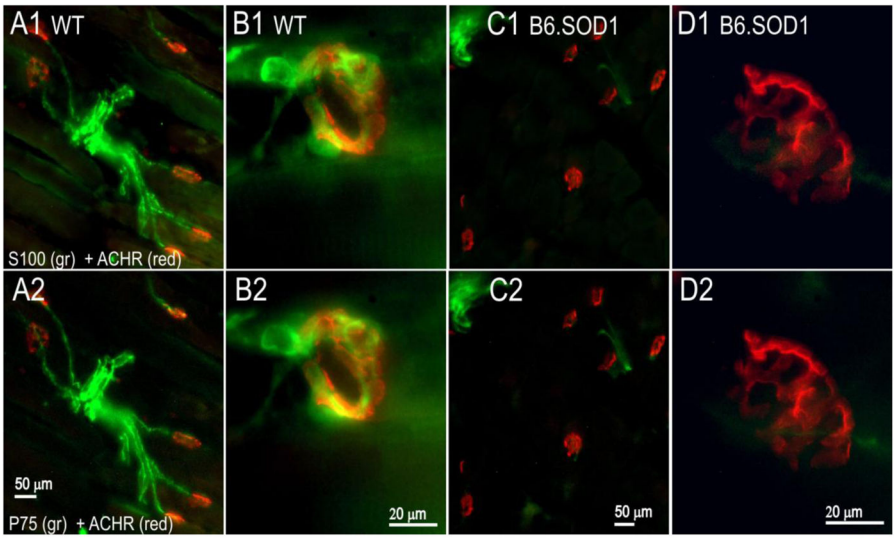

Figure 2.

P75 labeling appears only where S100 is expressed 4d after P30 sciatic crush denervation. A–D, top row, S100 + ACHR labeling. Bottom row, P75 + ACHR labeling. Panels demonstrate S100 and P75 labeling in relation to endplate ACHR labeling for the same tissue sections. A1–2. WT MG endplate zone (from Fig 1D). P75 and S100 label identically in preterminal regions and over endplates 4d after denervation. B1–2. High magnification images (100x) of WT MG NMJ showing similar pattern of P75 and S100 labeling at endplate. C1–2. B6.SOD1 MG endplate zone 4d after denervation. In this case, some P75 and S100 colabeling can be seen, but where S100 labeling is absent over endplates and in preterminal regions, P75 labeling is also absent. D1–2. High magnification images (100x) of B6.SOD1MG NMJ showing absence of P75 and S100 labeling.

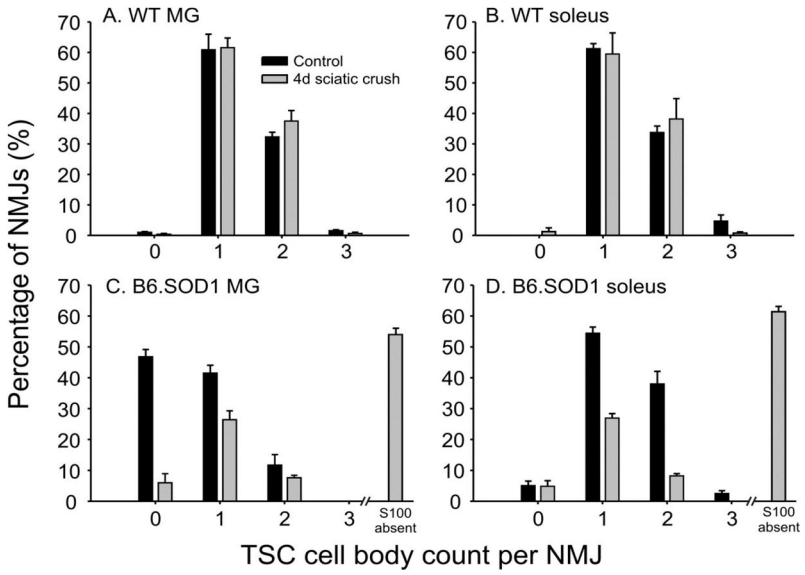

Figure 3.

P30 TSC cell count per NMJ 4d after sciatic crush denervation. TSC cell bodies were identified at a magnification of 100x by S100 + DAPI colabeling, and counts at individual NMJs were obtained. A. TSC counts for control WT MG NMJs and for 4d after sciatic nerve crush denervation. B. TSC counts for control WT soleus NMJs and for 4d after sciatic nerve crush denervation. No significant differences in between WT control and post-denervation distributions were observed (Pearson chi-square, $p > 0.05$). C. TSC counts for control B6.SOD1 MG NMJs and for 4d after sciatic nerve crush denervation. All control NMJs were fully covered by S100 labeling but many lacked TSC cell bodies and were covered by the processes of SCs with cell bodies located proximally along the preterminal axon (Carrasco et al., 2016). As indicated by the vertical bar on right-hand side of C, a majority (~ 60%) of B6.SOD1 NMJs lose S100 coverage 4d after denervation (see Fig 1), leaving about 40% of NMJs partially S100 covered. Average percentage of TSC counts from these NMJs are shown by the gray vertical bars; these bars total about 40% to emphasize that they represent a minority of NMJs 4d after denervation. These data show that TSC cell bodies can still be identified at a majority (ca 85%) of these partially S100 covered B6.SOD1 NMJs 4d after denervation. D. TSC counts for control B6.SOD1 soleus NMJs and for 4d after denervation. All control NMJs were fully S100-covered and only 5% lacked TSC cell bodies and were covered by the processes of remotely-located SCs. Similar to P30 B6.SOD1 MG NMJs, most soleus NMJs lose S100 labeling after denervation (Fig 1), so TSC data are shown only for the approximately 40% that retained some S100 labeling. These data show that TSC cell bodies remain identifiable at about 35% of soleus NMJs 4d after denervation.

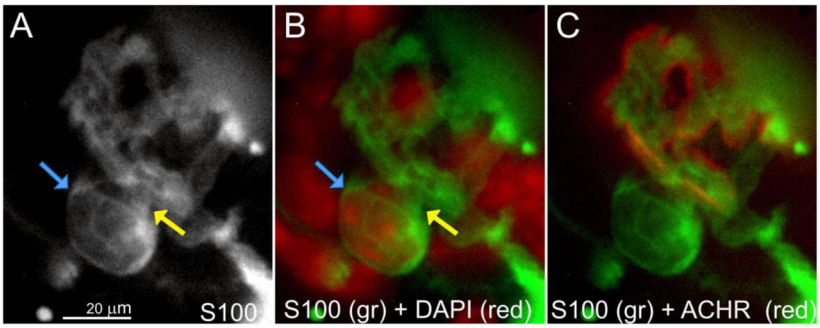

Figure 4.

B6.SOD1 soleus TSCs after sciatic crush denervation. Images illustrate a soleus endplate labeled for S100 (A), S100 + DAPI (B) and DAPI + ACHRs (C), observed 24 hrs after denervation when S100 labeling for TSCs remained relatively intact. S100/DAPI colabeled nucleus (blue arrows) appears to be attached by slender processes (A, B, yellow arrows) to adjacent endplate S100 processes, and appeared elevated from the endplate while varying the focal plane. Following a survey of more than 200 NMJs in 2 soleus muscles, this case was the best candidate example found in which a B6.SOD1 TSC appeared to be lifting off endplates soon after denervation.

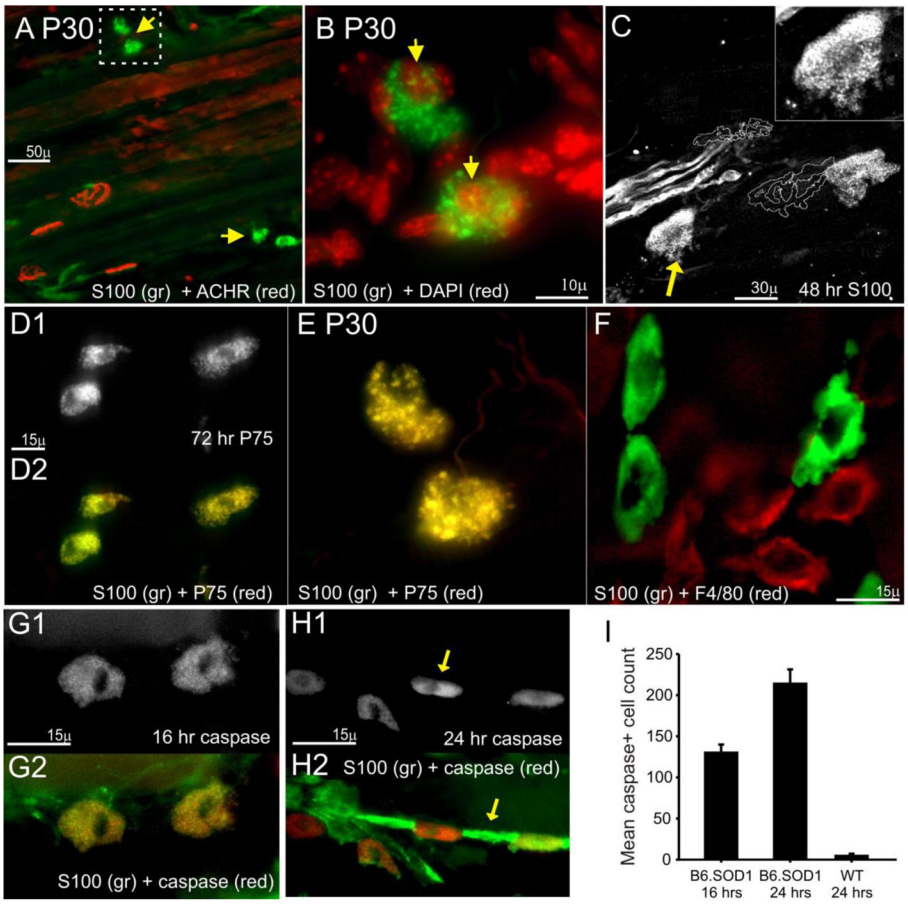

Figure 5.

Large S100+, P75+ cells increase in number and label for activated caspase-3 after sciatic crush denervation in B6.SOD1 muscles. A. Low magnification view of a P30 B6.SOD1 MG NMJ field 4d after sciatic crush denervation and labeled for S100 and ACHRs. Although no S100 labeling can be seen over endplates and elsewhere in this field, several brightly labeled cells can be seen nearby (yellow arrows). B. Higher magnification view of outlined area in A. DAPI-S100 colabeling demonstrates nuclei (yellow arrows). Characteristic features of these cells are the inclusion of particles brightly labeled for S100 and apparent discontinuities along the cell perimeter. C. P60 B6.SOD1 MG NMJs labeled for S100 (white) 48 h after denervation. ACHR-rich endplates are represented by white outlines. Endplates show no S100 labeling while remaining S100+ cells located away from endplates appear to be fragmenting. Upper right, detail of S00+ cell (yellow arrow) showing apparent fragmentation and small, brightly labeled circular particles. D–E. S100+ cells colabel for P75. D. Examples from P60 MG muscle 72 hrs after sciatic crush denervation labeled for P75 (D1) and colabeled for S100 (D2). E. Same cells shown in B colabeled for P75. Complete P75-S100 colabeling indicated by dominant yellow color in D and E, suggesting that these cells are SCs. F. P60 B6.SOD1 MG. S100-labeled cells (green) show no colabeling with F4/80 (red), a marker for macrophages while macrophages show no labeling for S100. G1. P60 B6.SOD1 S100+ cells located in preterminal area of B6.SOD1 MG muscle 16 hrs after crush denervation labeling positive for activated caspase-3. D2.

Activated caspase-3 (red) colabeling with S100 (green) demonstrating that caspase-3+ cells are SCs. H1–2. Asynchronous appearance of activated caspase-3 among contiguous SCs 24 hrs after sciatic crush. H1. Activated caspase-3 labeling only. H2. Overlay with S100 labeling (green). Images show closely-grouped cells labeled primarily for activated caspase-3 (H1, arrow), cells labeled only for S100 (H2, arrow) and other cells with graded colabeling. The predominantly linear arrangement suggests that these cells were may have been associated with axons prior to denervation. I. Mean (+ 1 SEM) counts of activated caspase-3+ cells in P60 B6.SOD1 MG muscles 16 and 24 hrs after sciatic crush. Cells labeling for activated caspase-3 were counted in 50 μm sections taken every 150 μm of MG muscle depth. In all cases, N = 3. In B6.SOD1 MG muscles, the mean counts increased from 16 to 24 hrs post crush. At 24 hrs, counts were significantly greater than in WT MG muscles, which showed a small number of caspase-3+ cells. Caspase-3+ cells in WT muscles were generally interspersed along lines and arranged similarly to that shown in panel H.

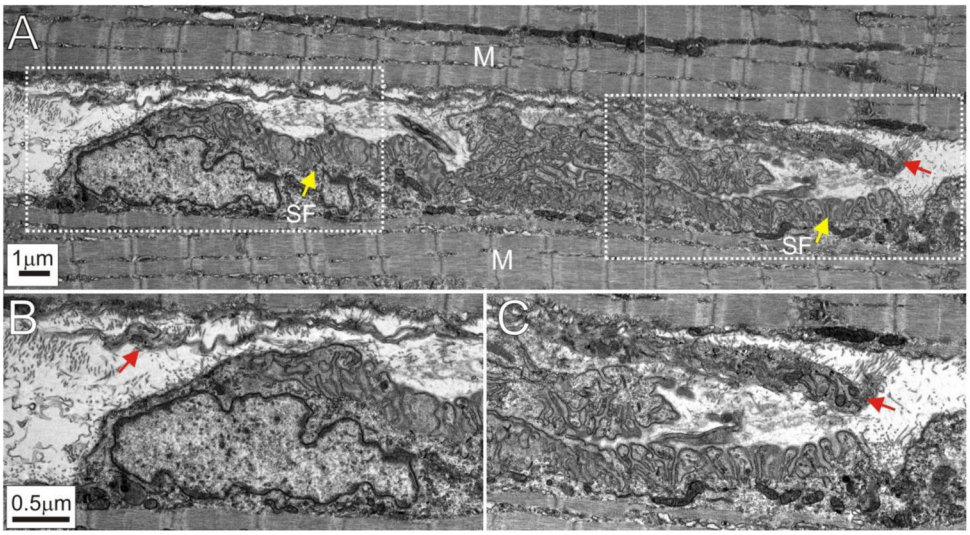

Figure 6.

Electron microscopy of a P45 B6.SOD1 MG endplate denervated 7d earlier. A. Panel shows the entire longitudinal extent of an endplate interposed between muscle (M). Yellow arrows indicate endplate secondary folds (SF). Because of denervation 7d earlier, no axons or nerve terminals are visible. B. Enlarged leftmost area indicated by interrupted white line shown in A. Only fibrils and other cellular debris can be seen overlying the secondary folds. A portion of an unidentified, ribbon-like structure which runs the length of the endplate may also be seen located above the endplate (red arrow). C. Enlarged rightmost area indicated by interrupted white line shown in A. Red arrow indicates rightmost extent of unidentified, ribbon-like structure. Note that the spaces between secondary folds and the nearest structures are filled with debris.

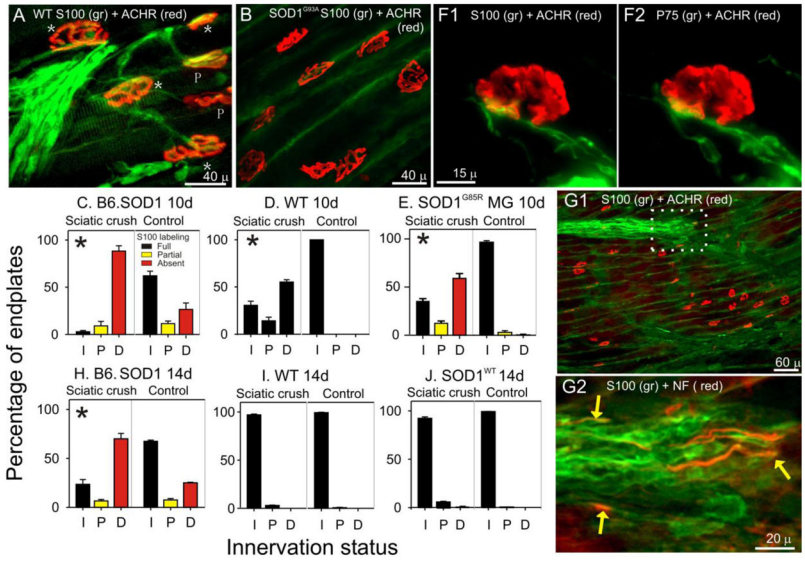

Figure 7.

NMJ S100 coverage and innervation 10 and 14d after sciatic crush denervation at P60. A. WT MG endplates 10 days after sciatic crush. Stars (*) indicate fully innervated endplates, P indicates partially innervated endplate. The extent of NMJ innervation was judged by assessing the extent to which labeling for neurofilaments (NF) extended into endplates. In this panel, ACHR-rich endplates are completely covered by S100 labeling (green) for TSCs as well as are preterminal SCs. All WT MG endplates were fully covered by S100 labeling independent of innervation status. B. B6.SOD1 MG endplates labeled for S100 and ACHRs 10 days after sciatic crush. No NF labeling (not shown) was observed at these ACHR-rich endplates or in the immediate preterminal regions demonstrating denervation. In this field, neither endplates nor preterminal regions exhibited S100 labeling for TSCs or for SCs. Green label reflects background labeling located between muscle fibers. C–E. Charts show mean percentage of NMJs for each of 3 innervation categories (I, innervated; P, partially innervated; F, fully innervated) at 10d after denervation compared between sciatic crush denervated and contralateral, control MG muscles for various data groups. Bar colors designate NMJ S100 coverage status; red bars indicate absence of labeling, yellow bars indicate partial coverage, black bars indicates full coverage. Asterisks placed in sciatic crush denervation side distributions indicate that sciatic crush and contralateral, control distributions differed significantly (Pearson chi-square, $p < 0.01$). At 10d, both B6.SOD1 (C) and WT MG (D) innervation remained significantly different from control sides but reinnervation of WT muscle appeared to be more progressed. All denervated B6.SOD1 MG NMJs remained completely uncovered by S100 labeling. As described in Results, $SOD1^{G85R}$ MG muscles (N = 2) were denervated and examined 10d later. The results (E) showed that denervated NMJs lacked S100 labeling, similar to results from B6.SOD1 (C). F. Example of S100 (F1) and P75 (F2) colabeling at an B6.SOD1 MG endplate 10 days after sciatic crush. Although SC processes can be seen approaching the endplate, the absence of both labels over the endplate indicates the absence of SC NMJ coverage. G1. Lower magnification view of B6.SOD1 MG endplate band labeled for S100 and ACHRs. No S100 labeling is observed over endplates or in preterminal regions. In the upper part of the panel,

an S100+ group of SC processes can be seen demonstrating the nearby presence of SCs. G2. White outlined region in B2 labeled for S100 (green) and NF (red). Regenerating axons (yellow arrows) can be seen in close association with SC processes but extending no further than the leading edge of S100 labeling. H–J. Charts show mean percentage of NMJs for each of 3 innervation categories at 14 after denervation. By 14d, WT MG (I) is essentially reinnervated whereas B6.SOD1 MG remains mostly denervated (H). This indicates that reinnervation of B6.SOD1 muscles is slowed compared with reinnervation of WT muscle. J. MG muscles from SOD^{WT} mice (N = 4) were denervated and NMJ innervation and S100 coverage studied 14d later. Reinnervation was essentially identical to that observed in WT MG after 14d thus demonstrating that overexpression of mutated protein does not underlie denervation effects seen at B6.SOD1 MG NMJs.